Barley α-amylase bound to its endogenous protein inhibitor BASI: crystal structure of the complex at 1.9 Å resolution

François Vallée[1†], Anders Kadziola[1‡], Yves Bourne[1], Michel Juy[1§], Kees W Rodenburg[2#], Birte Svensson[2] and Richard Haser[1§*]

Background: Barley α-amylase is a 45 kDa enzyme which is involved in starch degradation during barley seed germination. The released sugars provide the plant embryo with energy for growth. The major barley α-amylase isozyme (AMY2) binds with high affinity to the endogenous inhibitor BASI (barley α-amylase/subtilisin inhibitor) whereas the minor isozyme (AMY1) is not inhibited. BASI is a 19.6 kDa bifunctional protein that can simultaneously inhibit AMY2 and serine proteases of the subtilisin family. This inhibitor may therefore prevent degradation of the endosperm starch during premature sprouting and protect the seed from attack by pathogens secreting proteases.

Results: The crystal structure of AMY2 in complex with BASI was determined and refined at 1.9 Å resolution. BASI consists of a 12-stranded β-barrel structure which belongs to the β-trefoil fold family and inhibits AMY2 by sterically occluding access of the substrate to the active site of the enzyme. The AMY2–BASI complex is characterized by an unusual completely solvated calcium ion located at the protein–protein interface.

Conclusions: The AMY2–BASI complex represents the first reported structure of an endogenous protein–protein complex from a higher plant. The structure of the complex throws light on the strict specificity of BASI for AMY2, and shows that domain B of AMY2 contributes greatly to the specificity of enzyme–inhibitor recognition. In contrast to the three-dimensional structures of porcine pancreatic α-amylase in complex with proteinaceous inhibitors, the AMY2–BASI structure reveals that the catalytically essential amino acid residues of the enzyme are not directly bound to the inhibitor. Binding of BASI to AMY2 creates a cavity, exposed to the external medium, that is ideally shaped to accommodate an extra calcium ion. This feature may contribute to the inhibitory effect, as the key amino acid sidechains of the active site are in direct contact with water molecules which are in turn ligated to the calcium ion.

Addresses: [1]Architecture et Fonction des Macromolécules Biologiques, UPR 9039, Institut de Biologie Structurale et Microbiologie, CNRS, 31 Chemin Joseph Aiguier, 13402 Marseille cedex 20, France and [2]Department of Chemistry, Carlsberg Laboratory, Gamle Carlsberg Vej 10, DK-2500 Copenhagen Valby, Denmark.

Present addresses: [†]Division of Biochemistry Research, The Hospital for Sick Children, 555 University Avenue, Toronto, Ontario M5S1X8, Canada, [‡]Centre for Crystallographic Studies, Department of Chemistry, University of Copenhagen, Universitetsparken 5, DK-2100 Copenhagen Ø, Denmark, [§]Institut de Biologie et Chimie des Proteines, UPR 412, CNRS, 7 Passage du Vercors, 69367 Lyon cedex 07, France and [#]Department of Molecular and Structural Biology, Gustav Wieds Vej 10 Århus University, DK-8000 Århus C, Denmark.

*Corresponding author.
E-mail: r.haser@ibcp.fr

Key words: α-amylase, barley, bifunctional inhibitor, protein–protein interactions, X-ray crystallography

Received: 12 January 1998
Revisions requested: 4 February 1998
Revisions received: 9 March 1998
Accepted: 25 March 1998

Structure 15 May 1998, 6:649–659
http://biomednet.com/elecref/0969212600600649

Introduction

Amylases are hydrolytic enzymes which are widespread in nature, being found in animals, microbes and plants. These enzymes are involved in the degradation of α-1,4-linked sugar polymers, such as starch and glycogen, into oligosaccharides. The germinating barley seed contains two main isozymes of α-amylase, AMY1 and AMY2, both of which are involved in starch degradation to provide energy for the development of the plant embryo, as well as an endogenous inhibitor BASI (barley α-amylase/subtilisin inhibitor) [1–3]. While BASI has a high binding affinity for AMY2, it does not inhibit AMY1, although this isozyme is highly active during the initial hydrolysis of the starch granule. BASI is a bifunctional protein also inhibiting serine proteases of the subtilisin family [1]. BASI may, therefore, have two roles: to prevent the endogenous AMY2 from hydrolytic attack on starch during premature sprouting and to protect the seed against exogenous proteases produced by various pathogens and pests [4].

The effects of the endogenous inhibitor BASI on starch hydrolysis have been studied under various conditions [5]. The affinity of AMY2 for BASI is weakened with decreasing pH levels from pH 8.0 to pH 6.0 [6], and increasing ionic strength up to 200 mM [5]. The K_i of the inhibition has been reported to be 2.2×10^{-10} M at pH 8 and 37°C [6]. The results of inactivating chemical modification suggested that a specific arginine residue on the surface of BASI is critical for the inhibition of AMY2 [6]. A differential labeling experiment followed by sequence analysis identified four arginine residues ($Arg27_{BASI}$, $Arg107_{BASI}$, $Arg127_{BASI}$ and $Arg155_{BASI}$) to be protected against phenylglyoxal modification in the AMY2–BASI complex, as compared to free BASI [7]. As $Arg27_{BASI}$ is not conserved in

Figure 1

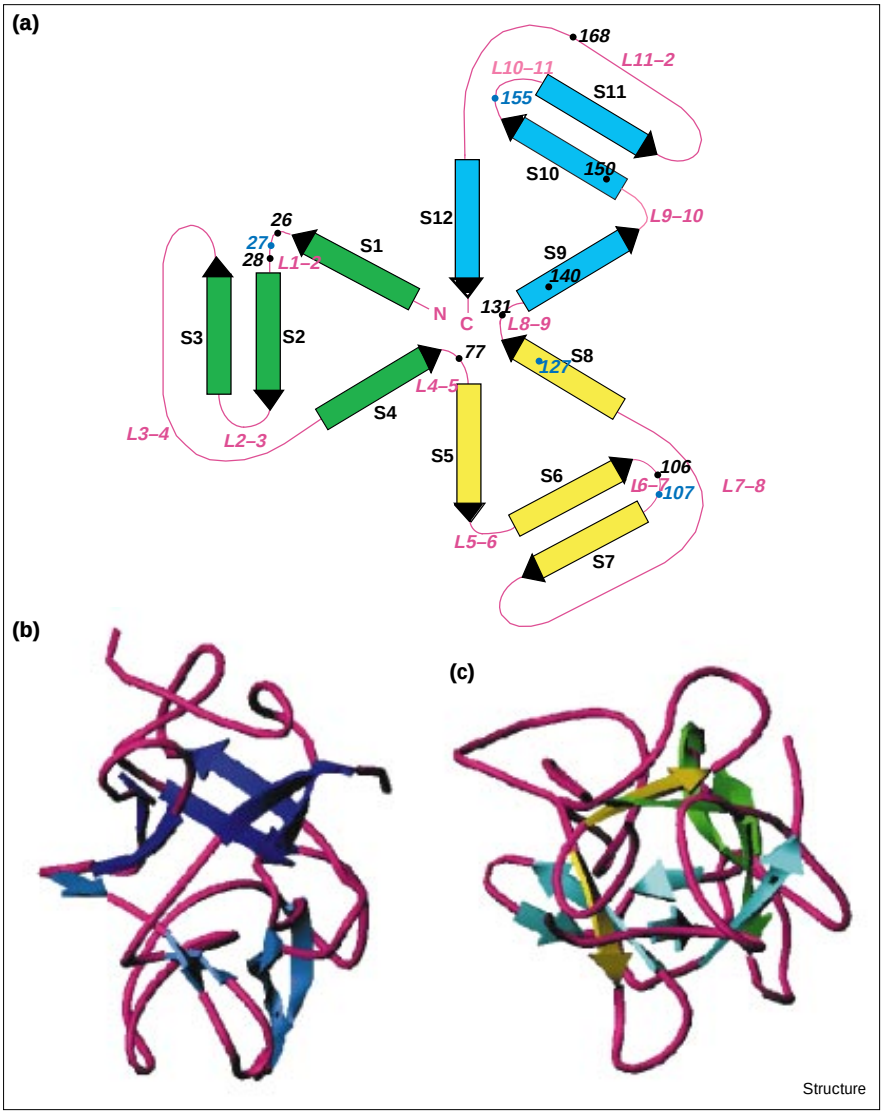

Overall fold of the BASI molecule. (a) Schematic fold of the BASI molecule showing the three groups of the β strands, S1 to S4, S5 to S8, and S9 to S12, colored in green, yellow and light blue, respectively. The 12 β strands identified are: S1, Asn19–Ser24; S2, Leu33–Gly38; S3, Arg41–Gln49; S4, Val60–Pro64; S5, Val80–Phe84; S6, His97–Ile98; S7, Val108–Ile109; S8, Phe186–Lys130; S9, Tyr139–Cys144; S10, Cys148–Phe154; S11, Phe163–Gly165; and S12, Val173–Ala178. Blue dots indicate the location of the four BASI arginine residues that are important for AMY2 binding. Black dots correspond to residues involved in direct hydrogen-bonding interactions with AMY2. (b) Ribbon diagram of the BASI structure; β strands of the β barrel and the hairpin loops are shown in purple and blue, respectively. (c) A view down the trefoil threefold symmetry axis with the three groups of β strands colored as in (a).

homologous inhibitors from different cereals and both $Arg107_{BASI}$ and $Arg127_{BASI}$ were only partially reactive, and thus not fully exposed [7], we suggested that $Arg155_{BASI}$ was the essential kinetically identified sensitive amino acid residue involved in AMY2 inhibition. This suggestion turns out to be in agreement with the present three-dimensional structure of the complex. Moreover, stopped-flow kinetic studies revealed that the AMY2–BASI complex results from a fast binding process yielding a rather loosely bound intermediate followed by a conformational change that tightens the complex [8].

The three-dimensional structures of several α-amylases have been solved, either in the free form or in complex with oligosaccharide or proteinaceous inhibitors: Taka-amylase A from *Aspergillus oryzae* [9,10]; porcine pancreatic α-amylase (PPA) [11,12]; AMY2 from barley [13,14]; human pancreatic α-amylase [15]; *Bacillus licheniformis* α-amylase [16]; human salivary α-amylase [17]; the complexes PPA–tendamistat [18] and PPA–α-AI (an α-amylase protein inhibitor from the bean *Phaseolus vulgaris)* [19]; and the psychrophilic α-amylase from *Alteromonas haloplanctis* in its native form and in complex with an inhibitor [20]. The crystal structures of AMY2 have been determined by X-ray crystallography in the native state, at 2.8 Å resolution, [13] and in complex with the pseudo-tetrasaccharide acarbose inhibitor [14]. AMY2 is a 403-residue single-chain protein with three free cysteine residues. The protein is folded into three distinct domains: a large central domain (domain A) forming a classical $(\alpha/\beta)_8$ barrel of the type common among all known α-amylases, many other amylolytic enzymes [21] and other proteins

of unrelated function [22]; a protruding loop domain (domain B; residues 89–152) structurally stabilized by three calcium ions; and a five-stranded antiparallel β sheet C-terminal domain (domain C).

BASI is a single-chain protein (181 residues) containing two disulphide bridges at positions Cys44–Cys90 and Cys144–Cys148. Sequence comparison has shown the existence of a very high degree of sequence identity between the bifunctional plant inhibitors of barley (BASI) and wheat (WASI) (92% identity), and to a lesser degree rice (RASI) (58% identity) and the Kunitz family trypsin inhibitors STI, WTI and ETI (around 25% identity) [23]. The three-dimensional structure of WASI has been reported in both its free state [24] and in complex with a serine protease, proteinase K [25].

Here we report the 1.9 Å resolution X-ray structure of the AMY2–BASI complex. The binding interface is characterized by a fully solvated calcium ion, which is not present in the AMY2 structure [13,14]. The extensive information obtained on the interface, the mode of action of this α-amylase inhibitor, and its high specificity for AMY2 as opposed to AMY1 are discussed.

Results and discussion

Structure of BASI

The BASI molecule displays the β-trefoil topology and measures approximately 47 Å × 39 Å × 27 Å (Figure 1), thus resembling several other β-trefoil structures such as those of WASI [24], interleukin 1α and β [26], histolactophiline [27], fibroblast growth factors [28], monofunctional trypsin inhibitors [23], and the ricin B chain [29]. The overall structure of the molecule shows an approximately threefold symmetry around the β-barrel axis. The three repeated units each consist of about 60 residues and contain four sequential β strands along with their connecting loops [30]. The hydrophobic core of the six-stranded β barrel is composed of β strands S1, S4, S5, S8, S9 and S12, along with a total of 18 hydrophobic internal residues which are essential to the stability of the fold. The hydrophobic core is closed at one end of the barrel axis by a triangular array consisting of the remaining β strands S2, S3, S6, S7, S10 and S11 in a hairpin arrangement, as already observed in Kunitz inhibitors and fibroblast growth factors [31,32]. The four cysteine residues Cys44, Cys90, Cys144 and Cys148 form two disulfide bridges Cys44–Cys90 and Cys144–Cys148, which are consistently present in the known structures of the Kunitz family inhibitors (ETI, WASI, STI) [23,24,33].

The AMY2–BASI complex interface

The AMY2 active-site region, which forms a large V-shaped depression on one side of the enzyme, involves the central domain A and part of domain B (Figure 2). BASI binds tightly to both of these domains, and its β-barrel axis is roughly perpendicular to the direction of the AMY2 $(\alpha/\beta)_8$-barrel axis. BASI sterically prevents access by the substrate to the AMY2 active site, but does not directly interact with the three essential catalytic residues, $Asp179_{AMY2}$, $Glu204_{AMY2}$ and $Asp289_{AMY2}$ [13,14,34], located at the bottom of the active-site depression. Remarkably, a large

Figure 2

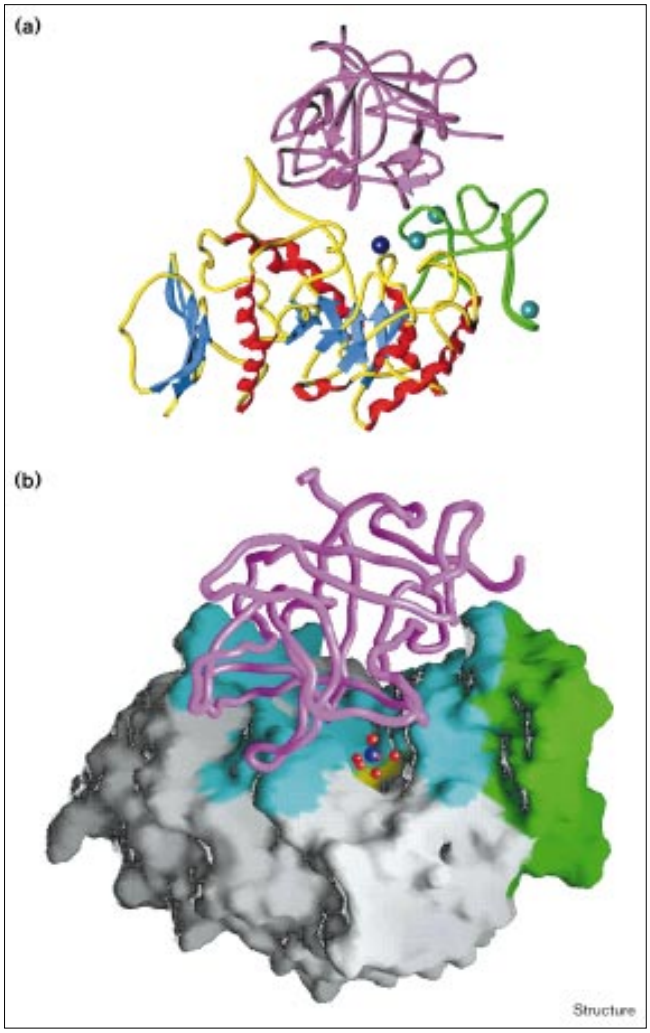

Overall view of the AMY2–BASI complex structure. (a) Ribbon diagram of the complex; β strands and α helices in AMY2 are shown in blue and red, respectively. AMY2 domain B and BASI are shown in green and purple, respectively. The three structural calcium ions which were previously observed in the AMY2 free structure [13] are shown in blue, whereas the fully solvated interfacial calcium ion, not present in free AMY2, is shown in dark blue. (b) Molecular surface representation of AMY2, colored to show residues buried to a 1.4 Å probe radius in cyan, non-buried residues in grey, the non-buried AMY2 domain B in green, and the AMY2 catalytic site in yellow. The backbone worm of the BASI molecule is shown with the same color-code and orientation as in (a). The interfacial calcium ion and the six liganded water molecules are displayed as blue and red spheres, respectively. (Figure generated using the program GRASP [63].)

cavity, in which a calcium ion is trapped, is created at the center of the AMY2–BASI binding interface (Figure 2).

Residues of the BASI β barrel within loops and secondary structure elements (loops L1–2, L4–5, L6–7, L8–9, L10–11, L11–12 and β strands S9 and S10) establish extensive hydrogen bonds, salt bridges and water-mediated contacts with residues of AMY2 situated in $(\alpha/\beta)_8$-barrel loops, β4–α4, β5–α5, α7a–α7b, and in helix α5 (Figure 3). There are 12 hydrogen bonds and two salt bridges between AMY2 and BASI. A total number of 48 residues (22 from AMY2 and 26 from BASI) establish contacts (including hydrogen bonds and van der Waals contacts) between the two proteins within 3.9 Å. In addition, a total number of 11 discrete water molecules, conserved in both complexes of the asymmetric unit, are buried within the interface and establish polar interactions between AMY2 and BASI (Table 1). This large number of water molecules mediating hydrogen bonds between AMY2 and BASI suggests that the solvent makes a large contribution to the steric complementarity of the two proteins, as found in other protein–protein complexes determined at high resolution [35,36].

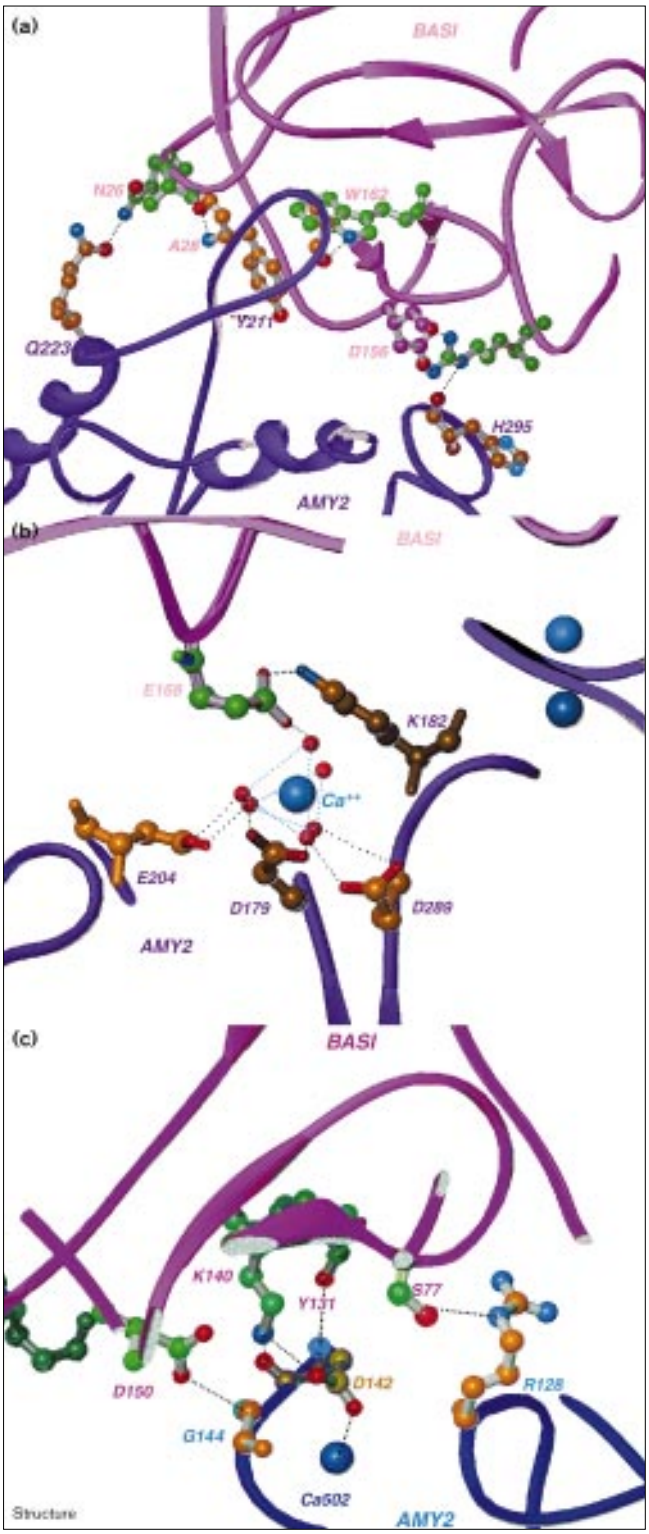

The total buried surface area in the AMY2–BASI complex is about 2355 Å^2 and comprises two distinct areas lying apart from the AMY2 catalytic site (Figures 2 and 3). This value for the buried surface is higher than those usually observed in other protein–inhibitor complexes [37] (excluding the PPA–α-AI and thrombin–inhibitor complexes [19,38]) and is in agreement with the low dissociation constant measured for the AMY2–BASI complex [6].

Comparison between free and complexed AMY2

No major structural differences were found to exist between the two AMY2 molecules present in the asymmetric unit, the root mean square (rms) deviation averaged over all Cα atoms was 0.23 Å. Moreover, pairwise superimposition of the Cα atoms of the free [13] and bound AMY2 molecules yielded an rms deviation of only 0.26 Å, indicating that the overall folding pattern is practically identical. The $Arg128_{AMY2}$ sidechain, which is located in domain B and participates in the binding interface, adopts a significantly different conformation in the free and bound forms, however.

Figure 3

Details of the three interacting regions between the AMY2 and BASI molecules. BASI and AMY2 are shown in light and dark purple with sidechains in green and brown, respectively. **(a)** The intramolecular hydrogen bonds between $Arg106_{BASI}$ and $Asp156_{BASI}$ are shown as blue dashed lines. An additional hydrogen bond involves $Gln223_{AMY2}$ and $Asn26_{BASI}$. **(b)** The central salt bridge between $Lys182_{AMY2}$ and $Glu168_{BASI}$ is represented with the fully solvated interfacial calcium and the AMY2 catalytic residues (Asp179, Glu204 and Asp289). **(c)** Interactions between AMY2 domain B and BASI. The central $Asp142_{AMY2}$ (in yellow) is bound to both a structural calcium ion (Ca502; seen in [13]) and to residues $Tyr131_{BASI}$ and $Lys140_{BASI}$. A salt bridge is established between $Asp142_{AMY2}$ and $Lys140_{BASI}$. Other polar interactions occur between $Gly144_{AMY2}$ and $Asp150_{BASI}$, and between $Arg128_{AMY2}$ and $Ser77_{BASI}$ (also see Table 1).

Table 1

All contacts in the AMY2–BASI complex.

Amino acid residues*		Hydrogen bonds between $AMY2_B$ and $BASI_D$ atoms†‡		
Enzyme residues	Inhibitor residues	Direct hydrogen bond	Distance (Å)	Water-mediated hydrogen bonds§
Arg128	Pro3, Pro4, Leu76, Ser77	Arg128 Nε↔Ser77 Oγ	2.83	Arg128 O ↔ W444↔Glu129 Oε1
Asp138	Gly133			Arg128 Nη1↔W460↔Glu129 Oε1
				Arg128 O↔W444↔Arg127 Nη2
Gly140, Ala141, Asp142	Ser132, Gly133, Tyr131	Asp142↔Tyr131 O	2.97	Asp142 O ↔W564↔Tyr131 O
Phe143, Gly144, Ala145	Ser132, Lys140, Met142	Asp142 O↔Lys140 Nζ	2.82	
	Cys148, Asp150	Asp142 Oδ2↔Lys140 Nζ	2.86	
		Gly144 N↔Asp150 Oδ1	2.91	
Phe180	Glu168, Tyr170			Glu204 Oε1↔W228↔Glu168 Oε2
Lys182	Tyr131, Glu168	Lys182 Nζ↔Glu168 Oε1	2.98	Lys182 Nζ↔W472↔Tyr170 O
Trp206	Glu168, Tyr170			
Ser208, Leu209, Ala210	Ala28, His29, Pro51	Tyr211 N↔Ala28 O	2.87	Tyr211 OH↔W325↔Arg155 O
Tyr211, Gly212, Gly213	Arg155, Trp162, Pro169			Ser208 Oγ↔W299↔Arg155 Nε
Gly215	Pro51, Arg155, Leu157	Gly215 O↔Trp162 Nε1	3.21	Gly215 O↔W233↔Arg155 O
Gln223	Asn26	Gln223 Oε1↔Asn26 Nδ2	3.32	
His295, Met296	Gly105, Arg106, Thr167	His295 O↔Arg106 Nε	2.80	Met296 O↔W485↔Glu168 O
	Glu168	His295 O↔Arg106 Nη1	2.83	
Pro298	Arg106, Asp156, Lys158			Pro298 O↔W308↔Asp156 Oδ2

*Contacts considered between 2.5 Å and 3.9 Å. †Contacts considered between 2.5 Å and 3.4 Å. ‡Subscripts B and D refer to one of the two independent AMY2–BASI complexes in the asymmetric unit. §W refers to numbered water molecules in the structure (water molecules binding to the interfacial calcium ion are not considered).

Upon analyzing the temperature factor (B) values between the free and bound AMY2 structures, in order to assess their mobility characteristics, a decrease in the B values was seen for almost all of the AMY2 interfacial residues. This observation is consistent with the idea that these residues undergo a conformational stabilization on binding to BASI. For example, the average B factor values of the $Lys182_{AMY2}$ and the $Arg128_{AMY2}$ sidechains were significantly lower in the AMY2–BASI complex (17.0 $Å^2$ and 31.2 $Å^2$, respectively) than in the free AMY2 structure (22.4 $Å^2$ and 39.9 $Å^2$, respectively).

Likewise, superimposition of the Cα atoms of the two BASI inhibitor molecules present in the asymmetric unit yielded an rms deviation of 0.31 Å in 177 out of 181 Cα atoms, indicating that the overall conformation of the two BASI molecules is nearly identical. Larger differences (of up to 4.5 Å) were observed only in the BASI loop which connects β strand S4 to S5 (residues 65–79); this loop is located on the opposite side to the AMY2-binding region. This loop was poorly defined in the electron-density map, probably due to the lack of intermolecular contacts in the crystal.

AMY2–BASI: a fast and tightly bound protein–protein complex

The recently described structures of the PPA–tendamistat [18] and PPA–α-AI complexes [19] throw light on the protein–inhibitor associations occurring in the α-amylase protein family. Comparisons between the three α-amylase–inhibitor complex structures showed a common feature: in the case of all three inhibitors, tendamistat, α-AI and BASI, steric hindrance prevents the substrate from reaching the catalytic site of the α-amylases. This functional aspect probably results from the tight binding in the three complexes: the dissociation constants of the AMY2–BASI, PPA–tendamistat and PPA–α-AI complexes being 2.2×10^{-10} M [6], 9×10^{-12} M [39] and 3.5×10^{-11} M [19], respectively. The lack of any significant conformational rearrangements of AMY2, a characteristic of AMY2–BASI complex formation, presumably contributes to the fast binding reaction, typically observed in several proteinase–inhibitor complexes [38]. This finding distinguishes AMY2–BASI from the PPA–α-AI complex in which a large number of conformational changes occur in a loop near the PPA catalytic site upon binding of the inhibitor [19].

BASI binding to AMY2 creates an interfacial calcium ion binding site

The refined structure of the AMY2–BASI complex unambiguously showed the presence of a completely solvated calcium ion at the center of the interface, which is not present in the structure of free AMY2 [13]. Surprisingly, this calcium ion does not bind directly to any of the neighboring acidic sidechains, as is usual for calcium-binding sites in proteins [40], but instead is stabilized by six ordered water molecules, with a trigonal biprismastic geometry (Figures 3 and 4; Table 2). Five of these water

Figure 4

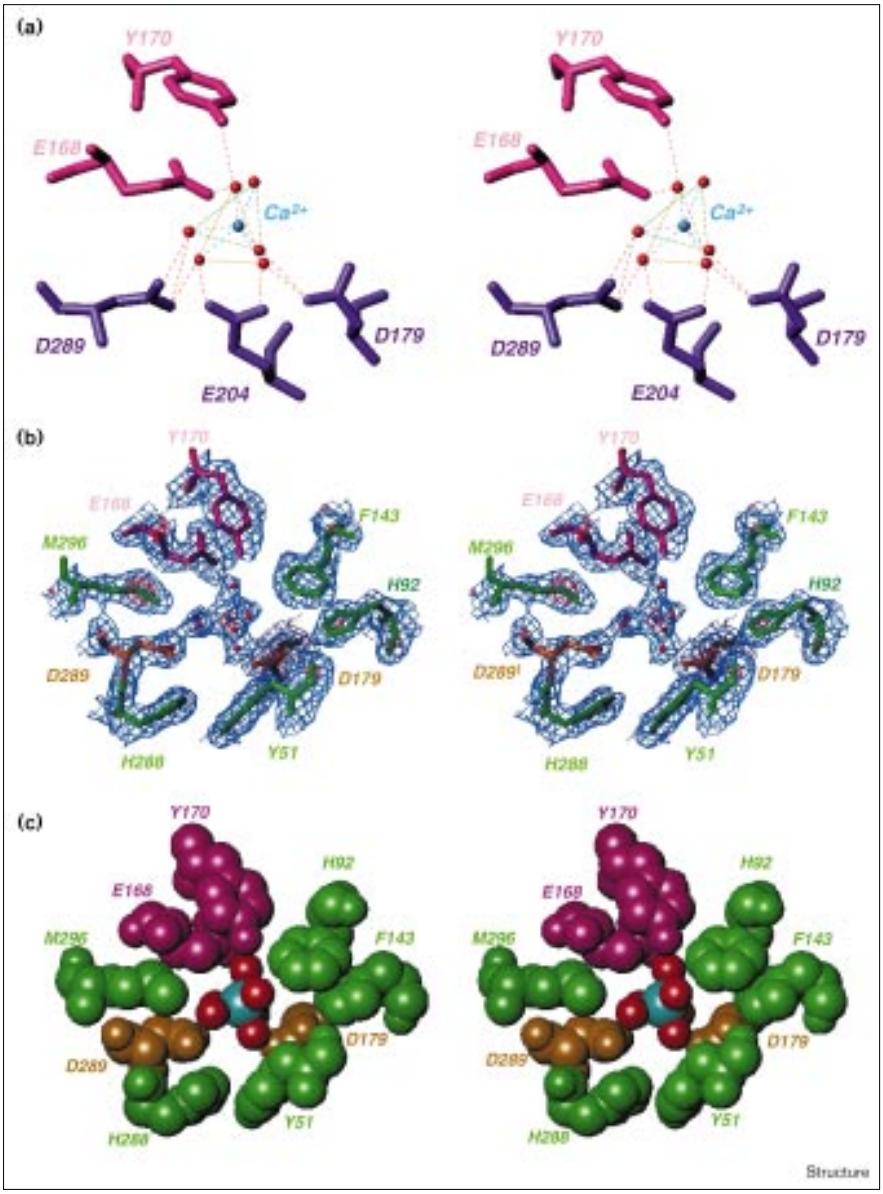

Details of the interfacial calcium ion binding site. (a) Stereoview of the calcium ion (blue) and its bound water molecules (red) with the surrounding AMY2 (purple) and BASI (magenta) sidechains $Tyr170_{BASI}$, $Glu168_{BASI}$, $Asp289_{AMY2}$, $Glu204_{AMY2}$ and $Asp179_{AMY2}$. Associated hydrogen bonds are shown as pink dashed lines. The yellow and green triangles help to visualise the trigonal biprismatic calcium coordination. (b) Stereoview of the 1.9 Å resolution simulated annealing F_o–F_c electron-density map, contoured at 1.2σ (blue) and 6σ (red), showing the interfacial calcium ion near the AMY2 catalytic cavity. The atoms found in this region (approximately 5% of the total number of atoms) were omitted from the calculations in the two AMY2–BASI complexes present in the asymmetric unit, and the remaining protein atoms were refined by simulated annealing before the final phase calculation. The BASI residues are labeled in pink and AMY2 residues are in green; AMY2 catalytic residues are shown in brown. Water molecules and the interfacial calcium ion are colored as in (a). (c) Stereoview CPK representation of the same region as in (b). Atoms are color-coded as in (b).

molecules are hydrogen bonded to carboxylate oxygen atoms of the surrounding catalytic site residues, $Asp179_{AMY2}$, $Glu204_{AMY2}$, $Asp289_{AMY2}$, and to oxygen atoms of $Glu168_{BASI}$ and $Tyr170_{BASI}$ (Figure 4). A sixth water molecule, which interacts only with the calcium ion, completes the calcium coordination sphere leading to a slightly distorted trigonal biprismatic arrangement of ligands around this ion. An overall comparison between the water molecule network in the active site of free and BASI-bound AMY2 suggests that the electrostatic field due to the calcium ion favors the formation of a water molecule network connected to the catalytic site, when BASI binds to AMY2.

The AMY2 domain B: a module controlling the isozyme specificity of BASI inhibition

Despite 80% sequence identity, the barley isozymes AMY1 and AMY2 exhibit different BASI-binding properties [1,5,41]. In contrast to AMY2, AMY1 is not inhibited by BASI [41] and experiments adding BASI in large excess to AMY1 indicate K_i to be greater than 1 mM (KWR and BS, unpublished data). It has been established that in several hybrids of AMY1 and AMY2 obtained by homologous recombination in yeast [42], the domain B (residues 89–152) of AMY2 is essential to BASI inhibition [41,43]. The isozyme hybrid *H161*, which contains AMY1 residues 1–161 and the complementary C-terminal region of AMY2

Table 2

Interfacial calcium-bound water molecules.

AMY2*	Water (B factor Å²)†	Water–calcium distances (Å)	Water (B factor Å²)†	BASI
Complex AMY_B–$BASI_D$				
Asp289 Oδ1	OW284 (27.8)	2.45		
Asp179 Oδ1	OW285 (30.2)	2.13		
Glu204 Oε2, Asp179 Oδ1	OW288 (24.6)	2.29		
Asp289 Oδ2, Glu204 Oε2	OW334 (26.0)	2.55		
		2.42	OW336 (27.2)	Glu168 Oε2, Tyr170 OH
	OW335 (42.6)	2.52		
Complex AMY_A–$BASI_C$				
Asp289 Oδ1	OW114 (31.3)	2.34		
Asp179 Oδ1	OW562 (31.7)	2.37		
Glu204 Oε1, Asp179 Oδ1	OW152 (22.1)	2.22		
Asp289 Oδ2, Glu204 Oε2	OW97 (27.9)	2.45		
		2.14	OW98 (28.8)	Glu168 Oε2, Tyr170 OH
	OW702 (27.9)	2.68		

*Subscripts A, B, C and D refer to the two independent AMY2 and BASI molecules of the asymmetric unit, respectively. †The B factor values are given in parentheses.

(residues 161–403), was insensitive to BASI inhibition. In contrast, hybrid *H90*, which contains AMY1 residues 1–90 and the complementary C-terminal region of AMY2 (residues 89–403), has practically identical biochemical properties to those observed with wild-type AMY2. Recent sequence analysis of three more hybrids, *H112*, *H116* and *H144*, with cross-over points within domain B, have shown that regions Leu117–Phe144, and to a lesser degree Ala145–Leu161, are critical for BASI binding to AMY2 [43]. A sequence comparison of AMY1 and AMY2, based on the three-dimensional structure of AMY2–BASI, showed that $Arg128_{AMY2}$ is the only charged residue at the binding interface which is not conserved in AMY1 (Figure 5). Another charged residue from domain B of AMY2, $Asp142_{AMY2}$, binds both to a calcium ion and to BASI (Figure 3) and is conserved in both isozymes. Biochemical studies of the mutant hybrids *H161* (Thr129→Arg/Lys130→Pro), *H90* (Arg129→Gln) and *H90* (Asp143→Asn) (AMY1 sequence numbering) supported the fact that the interactions between $Arg128_{AMY2}$ Nε and $Ser77_{BASI}$ Oγ and between $Asp142_{AMY2}$ Oδ2 and $Lys140_{BASI}$ Nζ are of great importance, but not essential to BASI binding [44]. The specificity of BASI for AMY2 therefore probably is a result of a combination of various interactions, as outlined below.

Firstly, domain B of AMY2 contains three proline residues, $Pro112_{AMY2}$, $Pro129_{AMY2}$ and $Pro137_{AMY2}$, which are located close to AMY2 residues involved in the calcium-binding sites ($Thr111_{AMY2}$, $Asp113_{AMY2}$, $Asp127_{AMY2}$ and $Asp138_{AMY2}$) and in the AMY2–BASI interaction ($Arg128_{AMY2}$). The three proline residues, which are not conserved in AMY1, are most probably critical to the conformation of domain B of AMY2 and hence to the recognition of BASI. Secondly, a putative disulfide bridge specific to domain B of AMY1 may contribute to the different behavior of the two isozymes towards BASI [45]. This bridge could involve residue $Cys95_{AMY1}$, which corresponds to Thr94 in AMY2, and either $Cys106_{AMY1}$ or $Cys125_{AMY1}$, both of which are conserved in the two isozymes [44]. Comparison of the distances from Cα of Thr94, Cys105 and Cys125 in AMY2, suggested that $Cys106_{AMY1}$ is the best candidate for disulfide bridge formation with $Cys95_{AMY1}$. In the structural model of AMY2, however, the Thr94 sidechain is oriented towards domain A. The formation of a disulfide bridge $Cys95_{AMY1}$–$Cys106_{AMY1}$ will therefore require a major conformational change in the $Cys95_{AMY1}$ sidechain towards the domain B in AMY1. This might contribute a conformational change to the AMY1 domain B which prevents BASI binding. Finally, sequence comparison outside domain B clearly showed that for the other critical sidechain, $Lys182_{AMY2}$/$Arg183_{AMY1}$, mutation in the binding interface of AMY2–BASI is close to the catalytic site but has no critical isolated impact on the BASI binding as the AMY1 mutant Arg183→Lys does not become sensitive to BASI [46]. Future information on the three-dimensional structure of AMY1 will help to elucidate reasons for the strict isozyme specificity of BASI for AMY2.

Involvement of the AMY2–BASI complex in the control of starch degradation

The synthesis and secretion of isozymes AMY1 and AMY2 in the germinating seed are differentially regulated at both the transcriptional and translational level [47–49]. Expression of genes encoding the different isozymes has been found to depend on the concentration of calcium ions and of the phytohormones found in the plant, gibberellic acid (GA_3) and abscisic acid (ABA) [47,50]. Unlike GA_3, ABA suppresses the expression of the α-amylase isozymes [51]. The effects of ABA in the unripe grain are twofold: firstly ABA has antagonistic effects on GA_3; and secondly

Figure 5

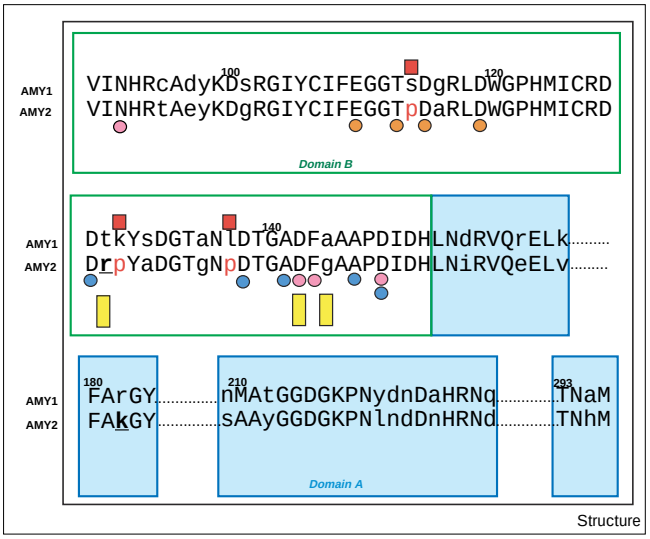

Sequence comparison of AMY1 and AMY2 relevant to the interface area of the AMY2–BASI complex. Residues involved in the interaction with BASI are indicated by yellow rectangles. Calcium ligands are marked by pink, orange and blue circles for Ca500, Ca501 and Ca502, respectively. Non-conservative substitutions are indicated with red squares. Bold and underlined residues designate sidechain substitutions between AMY1 and AMY2 for residues in interaction with BASI. Domain B is outlined in green, whereas domain A is shaded in blue.

stimulates the expression of embryogenic genes encoding, for example BASI [52]. The antagonistic regulation of the *de novo* synthesis of AMY and BASI proteins, as well as the AMY2 inhibition by BASI, imply that α-amylase activity is abolished both at the transcriptional and enzyme activity levels, this is perhaps significant in the case of premature sprouting. The role of ABA in response to environmental stress conditions and wounding [51,53] also suggests that BASI is a defense-related protein acting on pathogens, and that BASI complex formation with proteases counteracts pathogen infestation during the germination process. Owing to the high degree of sequence identity (92%) between WASI and BASI, the BASI–protease interactions may be modeled on the basis of the structure of the WASI–proteinase K complex [25]. A model of the ternary complex AMY2–BASI–proteinase K was therefore generated using the program TURBO-FRODO [54]. The model shows that the enzymes interact with BASI at very distinct, non-overlapping sites, which are found on opposite regions of the molecular surface of BASI. The BASI loop between β strands S5 and S6 (Figure 1a) seems to be the major structural determinant for recognizing the protease. However, further details and insights into the bifunctional role of BASI must await refinement of the WASI–proteinase K model and/or structure determination of the homologous BASI–protease complex, or even of a ternary AMY2–BASI–protease complex.

Biological implications

The regulation of starch degradation in the endosperm of the barley seed during germination involves a complex system of two α-amylase isozymes, AMY1 and AMY2, with distinctly different properties. Of these two isozymes, only AMY2 is inhibited by the endogenous bifunctional barley α-amylase/subtilisin inhibitor BASI.

Here we describe the three-dimensional structure of the AMY2–BASI complex, which throws light on the mechanism of α-amylase inhibition. BASI sterically blocks the catalytic cavity of AMY2, without binding directly to any of the three carboxylic acid residues involved in catalysis. The cavity created at the center of the protein–protein interface contains a completely solvated calcium ion located near the AMY2 catalytic residues.

Together with the results of biochemical analyses on isozyme hybrids, isozyme hybrid formation and site-directed mutagenesis studies, the present study provides a structural basis for understanding the different affinities of AMY1 and AMY2 for BASI. The interaction between the calcium-containing domain B of AMY2 and BASI supports the idea that the inhibition specificity results from a complex combination of several effects. Non-conservative substitutions and perhaps the different calcium affinities of AMY1 and AMY2 may influence the conformation of domain B and cause the lack of AMY1 sensitivity for BASI.

This highly specific binding may be necessary for the development of the germinating seed. The protein–protein association, which is involved in the control of sugar energy release to the plant embryo during growth, is combined with BASI's potential protease inhibition in response to various stress factors harmful to the germination process.

Materials and methods

Crystallization and data collection

AMY2 was purified from kilned barley malt (cultivar Menuet) [55] and BASI from barley seeds (cultivar Piggy) essentially as previously reported [6]. Crystallization trials were conducted using the hanging drop vapor diffusion method at room temperature (20°C) as previously described [56]. Crystals of the AMY2–BASI complex appeared within five days, by mixing an equal volume of the 1:1 complex solution (9.4 mg/ml) with the well solution containing 3–8% polyethylene glycol 6000, 10 mM MES pH 6.7 and 5 mM $CaCl_2$. X-ray diffraction data were collected at 20°C using a Rigaku RU200 rotating anode X-ray source operating at 40 kV and 80 mA and a MAR Research Imaging plate detector (Hamburg, Germany). The crystals are orthorhombic in space group $P2_12_12_1$, and the unit cell dimensions are a = 74.50 Å, b = 96.18 Å and c = 170.15 Å. There are two molecules of the complex in the asymmetric unit, which correspond to a volume of solvent equal to 45%. A preliminary data set was collected at 2.7 Å resolution with one crystal which was rotated a total of 110° using increments of 1°, and an exposure time of 800 s per degree. A second data set (550 frames), extending up to 1.9 Å resolution, was collected with one crystal using a crystal-to-plate distance of 80 mm and increments of 0.25°. The two data sets were reduced and scaled

Table 3

Summary of data collection and phasing statistics.

	Native 1	Native 2	$HgCl_2$	$Eu(NO_3)_3$
Resolution (Å)	2.7	1.9	2.8	2.7
Observed reflections	245 919	800 034	95 554	102 868
Unique reflections	31 211	95 528	24 555	29 170
Redundancy	7.8	8.4	3.9	3.5
R_{merge}*	6.7	10.5	10.5	9.4
R_{iso}			20.3	19.6
Number of sites			6	4
Phasing power (acentric/centric)			1.06/2.77	0.95/0.78
Highest resolution shell (Å)		2.1–1.9		
Completeness ($F_o > 2\sigma(F_o)$) (%)	95.5	91.3 (82.5†)	80.2	86.2

*$R_{merge} = \Sigma i,hkl \mid I(i,hkl) - < I(hkl) > \mid / \Sigma i,hkl < I(hkl) >$. †The number given in brackets denotes the respective value of the highest resolution shell.

Table 4

Crystallographic parameters of the refined structure.

Number of non-hydrogen protein atoms	9176
Number of water molecules	749
Overall R factor ($F_o > 1\sigma(F_o$°))	20.8
Overall R free	26.9
Mean B factor (Å^2)	
Amylase molecules	
molecule A	17.6*(19.3†)
molecule B	24.5*(25.5†)
BASI molecules	
molecule C	23.7*(25.5†)
molecule D	22.6*(24.8†)
Water molecules	
complex AC	30.1
complex BD	31.7
Rms deviation from ideal geometry	
bonds (Å)	0.007
angles (°)	1.45
dihedral angles (°)	25.3
improper angles	1.24
Rms variation in B factors (Å^2)	
bonds	2.1
angles	2.0

*Mean mainchain B factor (Å^2). †Mean sidechain B factor (Å^2).

using the XDS and XSCALE software programs [57], and then merged using the same program package. Details of the data collection statistics are shown in Table 3.

Molecular replacement

The 2.7 Å resolution data set (Table 3) was used for molecular replacement using the AMoRe software program [58] with the refined coordinates of the native AMY2 structure (PDB code 1AMY) as a search model [13]. Attempts to introduce the WASI structure into the search model were unsuccessful. Diffraction data in the resolution range of 8–3 Å were used in both the rotation and the translation function calculations. The two highest peaks, at 16.9σ and 16.3σ above the mean, were found with the rotation function. A correctly positioned AMY2 molecule was then used to locate the second molecule by means of the phased translation function, giving a correlation of 40.6%. The two AMY2 molecules were then subjected to rigid-body refinement with AMoRe [58], resulting in a correlation of 54.5% and an R factor of 41.6%. Further refinement with X-PLOR [59] using Powell conjugate-gradient energy minimization reduced the R factor value to 36.2% in the 10 Å to 2.7 Å resolution range. Subsequent $2F_o–F_c$ and $F_o–F_c$ electron-density maps identified the three calcium ions already found in the free AMY2 molecule, which were removed from the search model. This indicates that the two AMY2 molecules had been correctly positioned in the asymmetric unit. At this stage, attempts to build part of the BASI molecules using difference Fourier techniques were not successful, however. Therefore, it became necessary to try to obtain additional phase information from heavy-atom derivatives of the AMY2–BASI complex.

Heavy-atom derivative preparation and refinement – phase combination

Mercury and europium heavy-atom derivatives, which were successfully used for solving the native AMY2 structure [13], were prepared. Crystals of the AMY2–BASI complex were soaked in 10 mM $Eu(NO_3)_3$ for ten days, or in 0.01 mM $HgCl_2$ for a few hours. X-ray diffraction data were collected up to 2.8 Å and 2.7 Å resolution on the $HgCl_2$ and $Eu(NO_3)_3$ derivative crystals, respectively (Table 3). The difference Fourier maps $(F_{der}–F_{nat})e^{i\phi}$calc with phases ($\phi_{calc}$) calculated from the positioned AMY2 molecules showed six major binding sites for the Hg derivative and four sites for the Eu derivative, some at positions previously observed in the native AMY2 structure [13]. On the basis of these heavy-atom sites, phases were then generated with MLPHARE [60]. Structure factors based on the two positioned AMY2 molecules were calculated with SFALL [60], and the figures of merit derived from the calculated phases were obtained with the SIGMAA option PARTIAL [60]. Calculated phases were combined with the MIR phases using the option COMBINE of SIGMAA [60].

Model building and refinement

Model building was performed with the TURBO-FRODO software program [54]. Parts of the Cα chain of the two independent BASI molecules were identified using the BONES program with the improved electron-density maps, and for each of the two BASI molecules 50 residues out of a total of 181 residues were constructed. At this stage, the structure of the highly homologous protein WASI [24] was used to help with the construction of the BASI molecules. Subsequent cycles of simulated-annealing refinement using X-PLOR [59], alternating with manual rebuilding, made it possible to build the two BASI molecules independently. The refined structure at 2.7 Å resolution contains two AMY2–BASI complexes, six calcium ions and 360 water molecules and has an R factor of 15.3% based on all reflections with $F_o > 1\sigma(F_o)$. Two BASI loops with residues 65–79 and residues 110–126 had weak electron densities, and the positions of three sidechains within BASI loop 131–138 were unclear. In addition, Fourier difference electron-density maps showed an isolated peak at 6σ above the mean value and located at the center of the binding interface near the AMY2 catalytic residues, suggesting the presence of a fourth calcium ion.

Further refinement cycles were performed with the 1.9 Å resolution data set, where most of the positioning errors in the BASI model were corrected and solvent molecules were added. The position of $His132_{BASI}$ and $Ser137_{BASI}$ sidechains were switched, as observed in the WASI structure [24]. The sidechain $Val136_{BASI}$ was rotated approximately 180° around the mainchain axis, and residue 135 was also repositioned. The presence of two interfacial calcium ions, already suggested by the Fourier difference electron-density map at 2.7 Å resolution, was clearly confirmed. Further refinement cycles were performed with the eight independent calcium sites considered as neutral atoms, our experience showing that keeping the 2+ charge on the calcium atoms led to abnormally short distances with some of the calcium ligands. The 1.9 Å resolution refined model has a final R factor of 20.8% (on the basis of all reflections in the 8 Å to 1.9 Å resolution range with $F_o>1\sigma(F_o)$), and the value of R_{free} [61] for 10% of reflections against which the model was not refined was 25.9%. The stereochemistry of the final model was

examined with PROCHECK [62], and 88.5% of the residues were located in the most favourable regions while the remaining residues were in allowed regions. An overlay of the two complexes in the asymmetric unit reveals a nearly identical backbone conformation reflected by a low overall rms deviation of 0.26 Å, using 583 Cα atoms for superposition. The crystallographic parameters of the refined structure are given in Table 4.

Accession numbers

The coordinates of the AMY2–BASI crystal structure have been deposited at the Brookhaven Protein Data Bank (entry code 1AVA) and will be available one year after the date of publication.

Acknowledgements

We are grateful to H Driguez and V Tran for stimulating discussions, and to G Pal for access to preliminary coordinates of the WASI–proteinase complex. We thank S Ehlers for the preparations of BASI and AMY2 isozyme and V Zamboni-Roig for technical assistance. This work was supported by the European Union Biotech Programme Framework 3 (grant BIO2-CT94-3008) and by the CNRS (Centre National de la Recherche Scientifique).

References

1. Mundy, J., Svendsen, I. & Hejgaard, J. (1983). Barley α-amylase/subtilisin inhibitor. Isolation and characterization. *Carlsberg Res. Commun.* **48**, 81-90.
2. Svendsen, I., Hejgaard, J. & Mundy, J. (1986). Complete amino acid sequence of the α-amylase/subtilisin inhibitor from barley. *Carlsberg Res. Commun.* **51**, 43-50.
3. Leah, R. & Mundy, J. (1989). The bifunctional α-amylase/subtilisin inhibitor of barley: nucleotide sequence and patterns of seed specific expression. *Plant Mol. Biol.* **12**, 673-682.
4. Garcia-Olmedo, F., Salcedo, G., Sanchez-Monge, R., Gomez, L., Royo, J. & Carbonero, P. (1991). Plant proteinaceous inhibitors of proteinases and α-amylases. *Oxford Survey of Plant Mol. Cell Biol.* **4**, 275-334.
5. Weselake, R.J., MacGregor, A.W. & Hill, R.D. (1985). Effect of endogenous barley α-amylase inhibitor on hydrolysis of starch under various conditions. *J. Cereal Sci.* **3**, 249-259.
6. Abe, J., Sidenius, U. & Svensson, B. (1993). Arginine is essential for the α-amylase inhibitory activity of the α-amylase/subtilisin inhibitor (BASI) from barley seeds. *Biochem. J.* **293**, 151-155.
7. Rodenburg, K.W., Varallyay, E., Svendsen, I. & Svensson, B. (1995). Arg-27, Arg-127 and Arg-155 in the β-trefoil protein barley α-amylase/subtilisin inhibitor are interface residues in the complex with barley α-amylase 2. *Biochem. J.* **309**, 969-976.
8. Sidenius, U., Olsen, K., Svensson, B. & Christensen, U. (1995). Stopped-flow kinetic studies of the reaction of barley α-amylase/subtilisin inhibitor and the high pI barley α-amylase. *FEBS Lett.* **361**, 250-254.
9. Swift, H.J., *et al*., & Wilkinson, A.J. (1991). Structure and molecular model refinement of *Aspergillus oryzae* (TAKA) α-amylase: an application of the simulated annealing method. *Acta Cryst. B* **47**, 535-544.
10. Brzozowski, A.M. & Davies, G.J. (1997). Structure of the *Aspergillus oryzae* α-amylase complexed with the inhibitor acarbose at 2.0 Å resolution. *Biochemistry* **36**, 10837-10845.
11. Qian, M., Haser, R. & Payan, F. (1993). Structure and molecular model refinement of pig pancreatic α-amylase at 2.1 Å resolution. *J. Mol. Biol.* **231**, 785-799.
12. Larson, S.B., Greenwood, A., Cascio, D., Day, J. & McPherson, A. (1994). Refined molecular structure of pig pancreatic α-amylase at 2.1 Å resolution. *J. Mol. Biol.* **235**, 1560-1564.
13. Kadziola, A., Abe, J., Svensson, B. & Haser, R. (1994). Crystal and molecular structure of barley α-amylase. *J. Mol. Biol.* **239**, 104-121.
14. Kadziola, A., Søgaard, M., Svensson, B. & Haser, R. (1998). Molecular structure of a barley α-amylase-inhibitor complex: implications for starch binding and catalysis. *J. Mol. Biol.* **278**, 205–217.
15. Brayer, G.D., Luo, Y. & Withers, S.G. (1995). The structure of human pancreatic α-amylase at 1.8 Å resolution and comparisons with related enzymes. *Protein Sci.* **4**, 1730-1742.
16. Machius, M., Wiegand, G. & Huber, R. (1995). Crystal structure of Ca^{2+} depleted *Bacillus licheniformis* α-amylase at 2.2 Å resolution. *J. Mol. Biol.* **246**, 545-559.
17. Ramasubbu, N., Paloth, V., Luo, Y., Brayer, G.D. & Levine, M.J. (1996). Structure of human salivary α-amylase at 1.6 Å resolution: implications for its role in the oral activity. *Acta Cryst. D* **52**, 435-446.
18. Wiegand, G., Epp, O. & Huber, R. (1995). The crystal structure of porcine pancreatic α-amylase in complex with the microbial inhibitor Tendamistat. *J. Mol. Biol.* **247**, 99-110.
19. Bompard-Gilles, C., Rousseau, P., Rougé, P. & Payan, F. (1996). Substrate mimicry in the active center of a mammalian α-amylase: structural analysis of an enzyme–inhibitor complex. *Structure* **4**, 1441-1452.
20. Aghajari, N., Feller, G., Gerday, Ch. & Haser, R. (1998). Crystal structures of the psychrophilic α-amylase from *Alteromonas haloplanctis* in its native form and complexed with an inhibitor. *Protein Sci.* **7**, 564-572.
21. Davies, G.J. & Henrissat, B. (1995). Structures and mechanisms of glycosyl hydrolases. *Structure* **3**, 853-859.
22. Reardon, D. & Farber, G.K. (1995). The structure and evolution of α/β barrel proteins. *FASEB J.* **9**, 497-503.
23. Onesti, S. & Blow, D.M. (1991). Crystal structure of a Kunitz-type trypsin inhibitor from *Erythrina caffra* seeds. *J. Mol. Biol.* **217**, 153-176.
24. Zemke, K.J., Müller-Farhnow, A., Jany, K.-D., Pal, G.P. & Saenger, W. (1991). The three dimensional structure of the bifunctional proteinase K/α-amylase inhibitor from wheat (PKI3) at 2.5 Å resolution. *FEBS Lett.* **279**, 240-242.
25. Pal, G.P., Kavounis, C.A., Jany, K.D. & Tsernoglou, D. (1994). The three-dimensional structure of the complex of proteinase K with its naturally occurring inhibitor PKI3. *FEBS Lett.* **341**, 167-170.
26. Swindells, M.B. & Thornton, J.M. (1993). A study of structural determinants in the interleukin-1 fold. *Protein Eng.* **6**, 711-715.
27. Habazetti, J., Gondol, D., Wiltscheck, R., Otlewski, J., Schleicher, M. & Holak, T.A. (1992). Structure of histolactophilin is similar to interleukin-1β and fibroblast growth factor. *Nature* **359**, 855-858.
28. Zhu, X., *et al*., & Rees, D.C. (1991). Three-dimensional structure of acidic and basic fibroblast growth factor. *Science* **251**, 90-93.
29. Rutenber, E. & Robertus, J.D. (1991). Structure of ricin B-chain at 2.5 Å resolution. *Proteins* **10**, 260-269.
30. McLachlan, A.D. (1979). Three-fold structural pattern in the soybean trypsin inhibitor (Kunitz). *J. Mol. Biol.* **133**, 557-563.
31. Murzin, A.G., Lesk, A.M. & Chothia, C. (1992). β-Trefoil fold patterns of structure and sequence in the Kunitz inhibitors-1β and 1α and fibroblast growth factors. *J. Mol. Biol.* **223**, 531-543.
32. Murzin, A.G., Lesk, A.M. & Chothia, C. (1994). Principles determining the structure of β-sheet barrels in proteins. (a) A theoretical analysis and (b) the observed structures. *J. Mol. Biol.* **236**, 1369-1400.
33. Blow, D.M., Janin, J. & Sweet, R.M. (1974). Mode of action of soybean trypsin inhibitor (Kunitz) as a model for specific protein–protein interactions. *Nature* **249**, 54-57.
34. Søgaard, M., Kadziola, A., Haser, R. & Svensson, B. (1993). Site-directed mutagenesis of histidine 93, aspartic acid 180, glutamic acid 205, histidine 290, and aspartic 291 at the active site and tryptophan 279 at the new starch binding site in barley α-amylase 1. *J. Biol. Chem.* **268**, 22480-22484.
35. Bhat, T., *et al*., & Poljak, R.J. (1994). Bound water molecules and conformational stabilization help mediate an antigen–antibody association. *Proc. Natl. Acad. Sci. USA* **91**, 1089-1093.
36. Buckle, M.B., Schreiber, G. & Fersht, A. (1994). Protein–protein recognition: crystal structural analysis of a barnase–barstar complex at 2.0 Å resolution. *Biochemistry* **33**, 8878-8889.
37. Janin, J. & Chothia, C. (1990). Structure of protein–protein recognition sites. *J. Biol. Chem.* **265**, 16027-16030.
38. Bode, W. & Huber, R. (1992). Natural protein proteinase inhibitors and their interaction with proteinases. *Eur. J. Biochem.* **204**, 433-451.
39. Vértesy, L., Oeding, V., Bender, R., Zepf, K. & Nesemann, G. (1984). Tendamistat (Hoe 467), a tight-binding α-amylase inhibitor from *Streptomyces tendae* 4158. *Eur. J. Biochem.* **141**, 505-512.
40. McPhalen, C.A., Strynadka, N.C.J. & James, M.N.G. (1991). Calcium-binding sites in proteins: a structural perspective. *Adv. Protein Chem.* **42**, 77-144.
41. Rodenburg, K.W., Juge, N., Guo, X.-J., Søgaard, M., Chaix, J.-C. & Svensson, B. (1994). Domain B protruding at the third β-strand of the (α/β) barrel in barley α-amylase confers distinct isozyme-specific properties. *Eur. J. Biochem.* **221**, 277-284.
42. Juge, N., *et al*., & Guo. X.-J. (1993). Comparison of barley malt α-amylase isozymes 1 and 2: construction of cDNA hybrids by *in vivo* recombination and their expression in yeast. *Gene* **130**, 159-166.

43. Juge, N., Rodenbug, K.W., Guo, X.-J., Chaix, J.-C. & Svensson, B. (1995). Isozyme hybrids within the protruding third loop domain of the barley α-amylase $(\beta/\alpha)_8$ barrel. Implication for BASI sensitivity and substrate affinity. *FEBS Lett.* 363, 299-303.
44. Rodenburg, K.W., *et al.*, & Svensson, B. (1995). Mutational analysis of residues determining the sensitivity of barley α-amylase 2 to the barley α-amylase/subtilisin inhibitor. Miami Bio/Technology Winter Symposia, Miami, Florida. *Protein Eng.* 8, 9.
45. Søgaard, M., Andersen, J.S., Roepstorff, P. & Svensson, B. (1993). Electrospray mass spectrometry characterization of post-translational modifications of barley α-amylase 1 produced in yeast. *Bio/Technology* 11, 1162-1165.
46. Matsui, I. & Svensson, B. (1997). Improved activity and modulated action pattern obtained by random mutagenesis at the fourth β-α loop involved in substrate binding to the catalytic $(\beta/\alpha)_8$-barrel domain of barley α-amylase 1. *J. Biol. Chem.* 272, 22456-22463.
47. Chandler, P.M., Zwar, J.A., Jacobsen, J.V., Higgins, T.J.V. & Inglis, A.S. (1984). The effects of gibberellic acid and abscisic acid on α-amylase mRNA levels in barley aleurone layers studies using an α-amylase cDNA clone. *Plant Mol. Biol.* 3, 407-418.
48. Bush, D.S. & Jones, R.L. (1988). Cytoplasmic calcium and α-amylase secretion from barley aleurone protoplasts. *Eur. J. Cell Biol.* 46, 466-469.
49. Jones, R.L. & Jacobsen, J.V. (1991). Regulation of synthesis and transport of secreted proteins in cereal aleurone. *Int. Rev. Cytol.* 126, 49-87.
50. Jacobsen, J.V. & Beach, L.R. (1985). Control of transcription of α-amylase and RNA genes in barley aleurone protoplasts by gibberellin and abscisic acid. *Nature* 316, 275-277.
51. Lin, L.S. & Ho, T. (1986). Mode of action of abscisic acid in barley aleurone layers. *Plant Physiol.* 82, 289-297.
52. Giraudat, J., *et al.*, & Vartanian, N. (1994). Current advances in abscisic acid action and signalling. *Plant Mol. Biol.* 94, 1557-1577.
53. Chandler, P.M. & Robertson, M. (1994). Gene expression regulated by abscisic acid and its relation to stress tolerance. *Annu. Rev. Plant Physiol.* 45, 113-141.
54. Roussel, A. & Cambillau, C. (1989). TURBO-FRODO. In *Silicon Graphics Geometry Partners Directory.* (Silicon Graphics eds.), pp. 77–78, Silicon Graphics Mountain View, CA.
55. Ajandouz, E.H., Abe, J., Svensson, B. & Marchis-Mouren, G. (1992). Barley malt α-amylase, purification, action pattern, and subsite mapping of isozyme 1 and two members of the isozyme 2 subfamily using *p*-nitrophenylated malto-oligosaccharide substrates. *Biochim. Biophys. Acta* 1159, 193-202.
56. Vallée, F., Kadziola, A., Bourne, Y., Abe, J., Svensson, B. & Haser, R. (1994). Characterization, crystallization and preliminary X-ray crystallographic analysis of the complex between barley α-amylase and the bifunctional α-amylase/subtilisin inhibitor from barley seeds. *J. Mol. Biol.* 236, 368-371.
57. Kabsch, W. (1988). Evaluation of single crystal X-ray diffraction data from a position-sensitive detector. *J. Appl. Cryst.* 21, 916-924.
58. Navaza, J. (1994). AMoRe: an automated package for molecular replacement. *Acta Cryst. A* 50, 157-163.
59. Brünger, A.T. (1992). X-PLOR, *Version 3.1. A system for X-ray Crystallography and NMR.* Yale University Press, New Haven, CT.
60. CCP4. (1994). The CCP4 suite: programs for protein crystallography. *Acta Cryst. D* 50, 760-763.
61. Brünger, A.T. (1992). Free R value: a novel statistical quantity for assessing the accuracy of crystal structures. *Nature* 355, 472-475.
62. Laskowski, R.A., MacArthur, M.W., Moss, D.S. & Thornton, J.M. (1993). PROCHECK: a program to check the stereochemistry of protein structures. *J. Appl. Cryst.* 26, 283-291.
63. Nicholls, A., Bharadwaj, R. & Honig, B. (1993). GRASP: graphical representation and analysis of surface properties. *Biophys. J.* 64, A166.